LETTERS

# Seismic and aseismic slip on the Central Peru megathrust

Hugo Perfettini[1,2,6,7], Jean-Philippe Avouac[3], Hernando Tavera[2], Andrew Kositsky[3,9], Jean-Mathieu Nocquet[4], Francis Bondoux[1,2,6], Mohamed Chlieh[1,4], Anthony Sladen[3], Laurence Audin[1,2,7], Daniel L. Farber[5,8] & Pierre Soler[1]

**Slip on a subduction megathrust can be seismic or aseismic, with the two modes of slip complementing each other in time and space to accommodate the long-term plate motions. Although slip is almost purely aseismic at depths greater than about 40 km, heterogeneous surface strain[1–8] suggests that both modes of slip occur at shallower depths, with aseismic slip resulting from steady or transient creep in the interseismic and postseismic periods[9–11]. Thus, active faults seem to comprise areas that slip mostly during earthquakes, and areas that mostly slip aseismically. The size, location and frequency of earthquakes that a megathrust can generate thus depend on where and when aseismic creep is taking place, and what fraction of the long-term slip rate it accounts for. Here we address this issue by focusing on the central Peru megathrust. We show that the Pisco earthquake, with moment magnitude $M_w = 8.0$, ruptured two asperities within a patch that had remained locked in the interseismic period, and triggered aseismic frictional afterslip on two adjacent patches. The most prominent patch of afterslip coincides with the subducting Nazca ridge, an area also characterized by low interseismic coupling, which seems to have repeatedly acted as a barrier to seismic rupture propagation in the past. The seismogenic portion of the megathrust thus appears to be composed of interfingering rate-weakening and rate-strengthening patches. The rate-strengthening patches contribute to a high proportion of aseismic slip, and determine the extent and frequency of large interplate earthquakes. Aseismic slip accounts for as much as 50–70% of the slip budget on the seismogenic portion of the megathrust in central Peru, and the return period of earthquakes with $M_w = 8.0$ in the Pisco area is estimated to be 250 years.**

Imaging the patchwork made by areas of faults that mostly slip during earthquakes (governed by a rate-weakening friction law) and areas that mostly slip aseismically (governed by a rate-strengthening friction law)[12], and then estimating the fraction of slip that is taken up by earthquakes is challenging for a number of reasons. First, the pattern may not be spatially stationary. Second, areas that seem to remain locked in the interseismic period may include rate-strengthening patches lying in the stress shadow of locked rate-weakening patches that would not creep much[4]. Finally, interplate earthquakes might rupture rate-weakening patches only partially, or could propagate into adjacent rate-strengthening areas. Thus, a detailed understanding of the physics governing the spatio-temporal distribution of slip along megathrusts remains elusive. Here we address this issue using geodetic observations of postseismic deformation following the $M_w = 8.0$ Pisco earthquake of 2007, the co-seismic source model of which is well constrained from InSAR (interferometric synthetic aperture radar) data, teleseismic data and tsunami modelling[13], and for which geodetic measurements of interseismic strain were acquired before the earthquake[14,15].

The earthquake occurred on 15 August 2007, and generated a tsunami which reached an elevation of up to 10 m in the epicentral area[13]. The earthquake ruptured the subduction interface along which the Nazca plate subducts beneath the South American plate at about 6 cm yr$^{-1}$ (Fig. 1). Similar interplate $M > 8.0$ earthquakes have occurred offshore South and Central Peru in 1604, 1687, 1746 and 1868[16]. The 2007 earthquake ruptured the same segment as broke in 1746. The rupture initiated north of Pisco and propagated towards the south, producing up to 8 m of slip parallel to the Nazca–South America plate convergence. The co-seismic model of the earthquake[13] shows that it broke two distinct asperities 60 seconds apart.

We installed a continuous global positioning system network of five stations (Fig. 1), which were in operation from 20 days after the mainshock. The data analysed here cover the time period until day 408 after the mainshock (see Supplementary Information for details). All horizontal displacements are trenchwards (Fig. 1). The largest postseismic displacements are observed at the two southernmost stations LAGU and GUAD, with about 10 cm of cumulative displacement. Station LAGU shows about 5 cm of uplift, while GUAD shows 2.5 cm of subsidence (see Supplementary Information), suggesting that station LAGU is located close to, or on top of, a creeping patch that does not extend beneath GUAD. Both localized slip on the megathrust (afterslip) and viscous relaxation of the mantle can contribute to postseismic relaxation. Here we model only the effect of afterslip, because mantle relaxation would produce a broader-scale deformation than seen in our data, and because afterslip is generally thought to dominate early postseismic relaxation[17]. The continuous global positioning system time series were thus inverted for slip on the megathrust on the basis of the theory of dislocation in an elastic half-space[18], using a principal component analysis-based inversion method[19] (see Supplementary Information for details).

We used a curved fault geometry consistent with the co-seismic model[13]. The dip angle increases continuously from 6° at 5 km depth near the trench, to 30° at about 50 km depth. We tested a variety of models in which the rake was left free and spatially variable, or fixed to the direction of plate convergence (67° E). We also varied the weight put on smoothing and conducted several tests to identify the robust features needed to account for the observations. These sensitivity tests show that the data require two high-slip patches, labelled A and B in Fig. 2. Between days 20 and 408, nearly 40 cm

[1]Institut de Recherche pour le Développement, 44 Boulevard de Dunkerque, 13572 Marseille cedex 02, France. [2]Instituto Geofisico del Perú, Calle Badajos 169, Urb. Mayorazgo, Ate, Lima, Peru. [3]Tectonics Observatory, Division of Geological and Planetary Sciences, California Institute of Technology, Pasadena, California 91125, USA. [4]GéoAzur, 250 Rue Albert Einstein, 06560 Valbonne, France. [5]Department of Earth and Planetary Sciences, University of California Santa Cruz, Santa Cruz, California 95064, USA. [6]Laboratoire de Géophysique Interne et Tectonophysique, Université Joseph Fourier/CNRS/IRD/LCPC, Observatoire des Sciences de l'Univers de Grenoble, BP 53, 38041 Grenoble cedex 9, France. [7]Laboratoire des Mécanismes de Transfert en Géologie, Université Paul Sabatier/CNRS/IRD, Observatoire Midi-Pyrénées, 14 Avenue Edouard Belin, 31400 Toulouse, France. [8]Lawrence Livermore National Laboratory, 7000 East Avenue, Livermore, California 94550, USA. [9]Ashima Research, Pasadena, 600 S. Lake Ave., Pasadena, California 91106, USA.

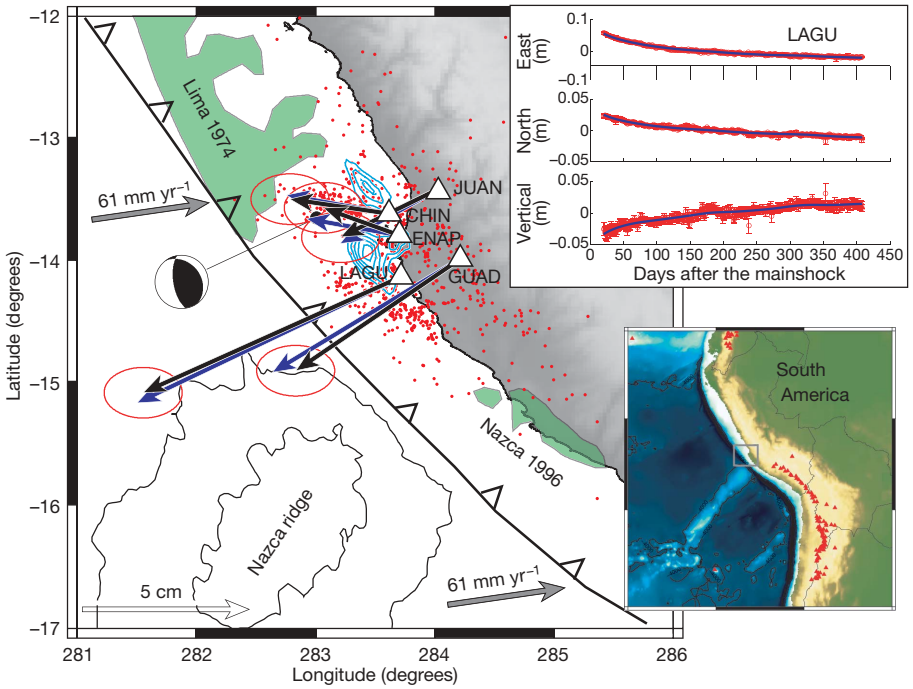


**Figure 1 | Seismotectonic setting of the South Peru megathrust.** Shown are co-seismic slip, aftershocks and postseismic displacements from the $M_w = 8.0$ Pisco earthquake in 2007. The focal mechanism shows the Global Centroid Moment Tensor solution (http://www.globalcmt.org/). The 2-m slip contour lines of the 2007 earthquake shown in cyan were derived from the joint analysis of InSAR, teleseismic and tsunami data[13]. Aftershocks (red dots) were located from the Instituto Geofísico del Perú (IGP) local seismic network. The rupture area of the $M_w$8.1, 1974 Lima earthquake was estimated from teleseismic data[28], and that of the $M_w$7.7, 1996 Nazca earthquake was derived from the joint inversion of InSAR and teleseismic waveforms[29]. Grey vectors show the Nazca plate motion relative to South America[14]. Black vectors show the horizontal postseismic displacements between days 20 and 408 after the mainshock, and the blue vectors show the modelled displacements. The time series of displacements recorded at LAGU, with $2\sigma$ uncertainties, is shown in the upper inset. The continuous curve shows the theoretical displacements predicted from the afterslip model shown in Fig. 2. The box in the lower inset represents the area of the main figure panel.

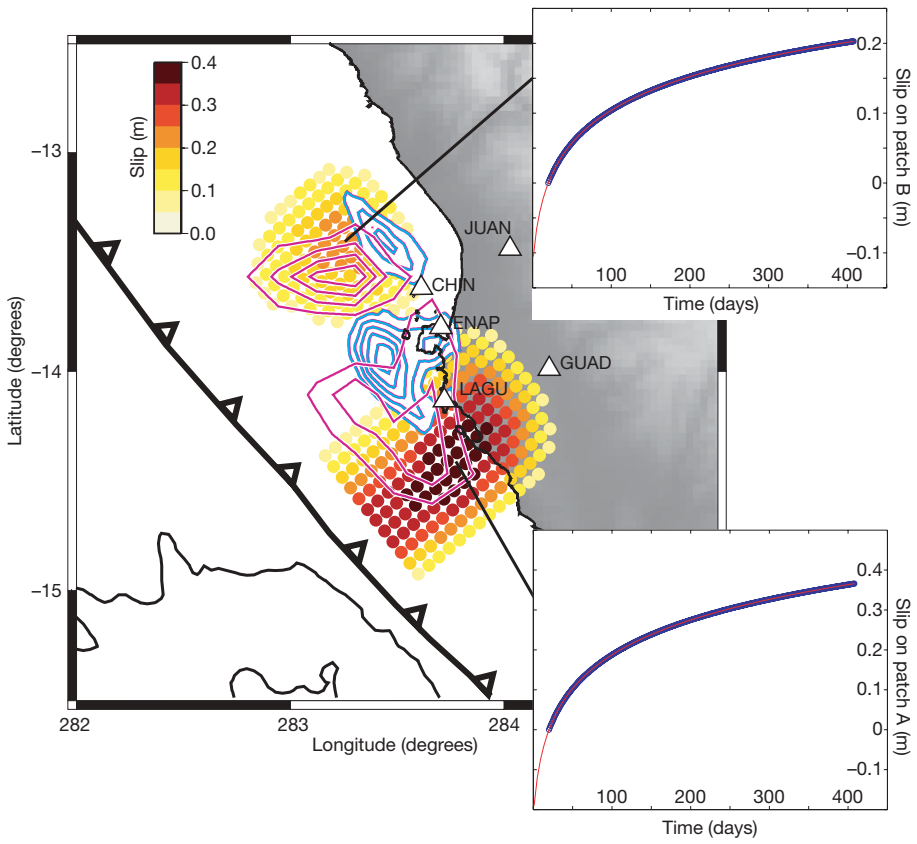


**Figure 2 | Fault slip derived from modelling of geodetic displacements between days 20 and 408 after the mainshock.** The model shown here assumes variable rake. Details regarding the weight put on smoothing and the three principal components selected in this model are given in the Supplementary Information. The 2-m slip contour lines of the 2007 earthquake are shown in cyan[13]. Pink contour lines show the density of aftershocks in the first month following the mainshock derived from the IGP catalogue. Insets show the slip at the centres of patches A and B, deduced from the inversion of geodetic measurements (blue circles). Red continuous lines show theoretical displacements predicted from rate-strengthening frictional sliding, assuming that frictional stress $\tau$ increases linearly with the logarithm of the sliding velocity $\dot{U}$, as observed in laboratory experiments[30]. According to this model, postseismic slip $U(t)$ evolves as[20] $U(t) \approx V_{pl} t_r \log\left[1 + (V^+/V_{pl} t_r)t\right]$. For patch A, the best fitting parameters are $t_r \approx 2.1$ years and $V^+/V_{pl} \approx 162$, assuming a value for the long-term velocity of the order of the convergence rate (that is, $V_0 = 62$ mm yr$^{-1}$; ref. 14). For patch B, we found $t_r \approx 1.2$ years and $V^+/V_{pl} \approx 90$, making the same assumptions as for patch A.

of slip occurred on patch A, and about 20 cm on patch B. We compared the time evolution of slip deduced from the inversion of the geodetic data with that predicted from a rate-strengthening frictional sliding law, which assumes that the frictional stress $\tau$ increases linearly with the logarithm of the sliding velocity $\dot{U}$ (ref. 20). The model fits the estimated postseismic slip remarkably well, yielding relaxation times $t_r$ of about 1.2 and 2.1 years for patches A and B (Fig. 2). According to this law, the ratio $V^+/V_{pl}$, where $V_{pl}$ is the long-term slip rate and $V^+$ is the sliding velocity on the fault directly after the earthquake, depends on the rheological parameter $A = d\tau/d\log \dot{U}$ (positive for rate-strengthening friction) and on the static Coulomb stress change induced by the mainshock ($\Delta$CFF)[20], according to the relation:

$$\Delta\mathrm{CFF} = A \log\left(V^+/V_{pl}\right)$$

We estimated the co-seismic Coulomb stress change based on the source model of the mainshock[13], and inferred $A \approx 0.20$–$0.59$ MPa at the centre of asperity A and $A \approx 0.22$–$0.67$ MPa at the centre of asperity B. These values are comparable to the 0.1–1 MPa range of estimates derived from other postseismic observations in various tectonic settings[11,20–24].

Our afterslip model amounts to a cumulative slip-potency (average slip $\times$ fault area) between 20 and 408 days of $3.45 \times 10^9$ m$^3$. Assuming a shear modulus of 50 GPa, this corresponds to a moment of $1.73 \times 10^{20}$ N m, equivalent to $M_w = 7.5$, representing 14% of the co-seismic moment released. The sensitivity tests given in the Supplementary Information yield a lower bound of $9.0 \times 10^{19}$ N m and an upper bound of $3.0 \times 10^{20}$ N m, corresponding to 7–28% of the co-seismic moment. Using the frictional afterslip model to estimate the cumulative moment during the first 20 days, we estimate that afterslip over the first 408 days released a geodetic moment of $3.33 \times 10^{20}$ N m ($M_w = 7.6$), representing about 28% of the co-seismic moment (the sensitivity tests yield a range of possible values between 22% and 41%). Given that the cumulative moment released by all aftershocks with $M_w > 4$ reported in the National Earthquake Information Center (NEIC) catalogue over the same period of time amounts to only $1.3 \times 10^{19}$ N m, about 90% of the observed postseismic deformation was aseismic. The 28% ratio of aseismic to seismic slip potency associated with the Pisco earthquake is comparable to similar estimations from a year of postseismic relaxation along other $M_w > 8$ megathrust earthquakes[11,25].

Data from a local seismic network also shows a clear spatial correlation between the distribution of aftershocks and the location of postseismic slip (Fig. 2), consistent with the notion that aftershocks are driven by afterslip[11,20,22,24,26,27]. Because the GPS stations were deployed 20 days after the mainshock, we could not test conclusively that the two processes are characterized by the same relaxation times.

Our modelling results show that the post- and co-seismic slip distributions complement each other (the small overlap might simply reflect the spatial smoothing employed in the inversion). This observation is consistent with the view that the shallow portion of the megathrust is paved with areas that are rate-weakening, within which earthquakes can nucleate and propagate, and areas that are rate-strengthening, within which slip is mostly aseismic. We therefore speculate that the two sub-events during the Pisco earthquake could reflect the effect of the intervening rate-strengthening patch (labelled B). Strikingly, the prominent aseismic patch (labelled A) coincides with the northern side of the Nazca ridge, where the 2007 rupture stopped. A number of $M > 8$ earthquakes have occurred, either north (1687, 1746) or south (1604, 1868) of Pisco in the past[16], but none seem to have ruptured across that particular patch of the megathrust. Therefore, we infer that this patch is a permanent barrier characterized by rate-strengthening friction, plausibly related to the subduction of the Nazca ridge. The intrinsically creeping character of the Peru megathrust in the area where the Nazca ridge subducts beneath the fore-arc is also visible from the pattern of interseismic strain. Modelling of the interseismic geodetic data recorded before the Pisco earthquake does indeed show low interseismic coupling in this area, while the rupture areas of the 2007 Pisco and 1974 Lima earthquakes coincide with higher coupling (Fig. 3 and Supplementary Information). The morphology of the fore-arc, characterized by an interruption of the fore-arc basins and a narrower distance from the trench to the coastline, probably also reflect the effects of the Nazca ridge.

With regard to the aseismic/seismic slip budget, the modelling of the interseismic deformation implies that 41–62% of the long-term interplate slip results from aseismic slip in the interseismic period (Fig. 3 and Supplementary Information). The remaining fraction of slip released during the earthquake cycle must result from transient seismic or aseismic slip. Assuming that the ratio between the moments released by afterslip and by seismic slip is about 28%, as estimated above, aseismic slip would contribute between 50% and 70% of the total slip (see Supplementary Information). This might still be an underestimate, because the possibility of spontaneous aseismic transients is ignored.

The interseismic coupling model suggests a moment deficit accumulation rate of $0.61 \times 10^{19}$ N m yr$^{-1}$ in the area that ruptured during the Pisco earthquake (latitude 13° S to 15° S, depth shallower than 40 km). At this rate, we estimate it would take about 250 years to accumulate a deficit of moment equivalent to the $1.5 \times 10^{21}$ N m released by co-seismic slip and afterslip associated with the Pisco earthquake. This estimate is close to the 261 years between the 2007 Pisco earthquake and the previous large megathrust earthquake in this area which occurred in 1746 (ref. 16).

To conclude, the Pisco earthquake ruptured two distinct asperities within patches that had remained locked in the interseismic period, and triggered aseismic afterslip on adjacent patches, including one that might actually separate the two seismic asperities. Afterslip released the equivalent of 28% of the co-seismic moment over one year, following a temporal evolution consistent with rate-strengthening frictional sliding. Aseismic slip on the seismogenic portion of the Peru megathrust between latitude 11° S and 16° S is estimated to account for a large

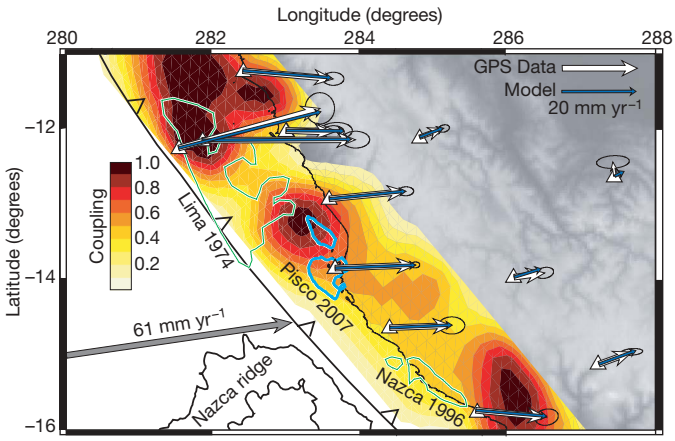


**Figure 3 | Comparison of interseismic coupling with the rupture areas of recent large earthquakes.** Rupture areas of the large interplate earthquakes as in Fig. 1. Also shown is the pattern of interseismic coupling, defined as $(1 - V_i/V_{pl})$, where $V_i$ is the interseismic slip rate, derived from modelling of geodetic data collected between January 1993 and March 2001, all referenced to stable South America[14,15]. Data (white vectors) were corrected for 5 mm yr$^{-1}$ of shortening across the Andes by least-squares adjustment of the Euler pole describing the long-term motion of the fore-arc with respect to South America. The rectangular fault model has a strike of 321° and dips 18° to the east. The inversion procedure is described in the Supplementary Information, and the modelled velocities are shown as light blue vectors. The small coupling near the trench may reflect the lack of resolution there, except in the north, where sea-bottom measurements are available[15]. This model shows that, on average over the study area, aseismic slip in the interseismic period accounts for about 38% to 59% of interplate slip at depths shallower than 40 km (the average interseismic coupling is between 0.41 and 0.62).

fraction of the slip budget. The dominant afterslip patch reflects the influence of the Nazca ridge, which seems to promote aseismic sliding and hence a locally low interseismic coupling, a result contrary to the common assumption that subducting bathymetric irregularities such as seamounts or ridges ought to increase seismic coupling. This area has repeatedly acted as a barrier to seismic rupture propagation. The megathrust appears to be paved with rate-strengthening and rate-weakening patches and the resulting pattern has a profound influence on its long-term seismic behaviour, as well as on individual earthquakes.

## METHODS SUMMARY

This study relies primarily on measurements of surface displacements from GPS geodesy. The surface displacements are used to infer the pattern of aseismic slip on the megathrust, based on the theory of elastic dislocations embedded in an elastic half-space[18]. The megathrust is modelled as 7 km × 7 km square dislocations. The inversions are regularized by minimizing the roughness of the solution calculated from the discrete Laplacian of the slip distribution. The time evolution of slip is retrieved using the principal component analysis-based inversion method of ref. 19. The time series are decomposed in principal components and each component is inverted for slip on the megathrust. The slip model is then obtained from linear combination of the minimum number of components required to fit the geodetic time series within uncertainties.

**Received 31 August 2009; accepted 26 March 2010.**


1. Savage, J. A dislocation model of strain accumulation and release at a subduction zone. *J. Geophys. Res.* **88,** 4984–4996 (1983).
2. Freymueller, J. & Beavan, J. Absence of strain accumulation in the Western Shumagin segment of the Alaska subduction zone. *Geophys. Res. Lett.* **26,** 3233–3236 (1999).
3. Mazzotti, S., Pichon, X. L., Henry, P. & Miyazaki, S. Full interseismic locking of the Nankai and Japan-West Kurile subduction zones: an analysis of uniform elastic strain accumulation in Japan constrained by permanent GPS. *J. Geophys. Res.* **105,** 13159–13159 (2000).
4. Burgmann, R., Kogan, M. G., Steblov, G. M., Hilley, G. & Levin, V. E. Interseismic coupling and asperity distribution along the Kamchatka subduction zone. *J. Geophys. Res.* **110,** doi:10.1020/2005JB003648 (2005).
5. Chlieh, M., Avouac, J.-P., Sieh, K., Natawidjaja, D. & Galetzka, J. Heterogeneous coupling of the sumatran megathrust constrained by geodetic and paleogeodetic measurements. *J. Geophys. Res.* **113,** doi:10.1029/2007JB004981 (2008).
6. Moreno, M., Klotz, J., Melnick, D., Echtler, H. & Bataille, K. Active faulting and heterogeneous deformation across a megathrust segment boundary from GPS data, South Central Chile (36°–39°s). *Geochem. Geophys. Geosyst.* **9,** doi:10.1029/2008GC002198 (2008).
7. Igarashi, T., Matsuzawa, T. & Hasegawa, A. Repeating earthquakes and interplate aseismic slip in the Northeastern Japan subduction zone. *J. Geophys. Res.* **108,** doi:10.1029/2002JB001920 (2003).
8. Suwa, Y., Hasegawa, A., Sato, T. & Tachibana, K. Interplate coupling beneath NE Japan inferred from three-dimensional displacement field. *J. Geophys. Res.* **111,** doi:10.1029/2004JB003203 (2006).
9. Hirose, H., Hirahara, K., Kimata, F., Fujii, N. & Miyazaki, S. A slow thrust slip event following the two 1996 Hyuganada earthquakes beneath the Bungo channel, southwest Japan. *Geophys. Res. Lett.* **26,** 3237–3240 (1999).
10. Miyazaki, S. *et al.* Modeling the rupture process of the 2003 September 25 Tokachi-Oki (Hokkaido) earthquake using 1-Hz GPS data. *Geophys. Res. Lett.* **31,** doi:10.1029/2004GL021457 (2004).
11. Hsu, Y.-J. *et al.* Frictional afterslip following the 2005 Nias-Simeulue earthquake, Sumatra. *Science* **312,** 1921–1926 (2006).
12. Bilek, S., Lay, T. & Ruff, L. Radiated seismic energy and earthquake source duration variations from teleseismic source time functions for shallow subduction zone thrust earthquakes. *J. Geophys. Res.* **109,** doi:10.1029/2004JB003039 (2004).
13. Sladen, A. *et al.* Source model of the 2007 $M_w$8.0 Pisco, Peru earthquake—implications for seismogenic behavior of subduction megathrusts. *J. Geophys. Res.* **115,** doi:10.1029/2009JB006429 (2010).
14. Kendrick, E., Bevis, M., Smalley, R. & Brooks, B. An integrated crustal velocity field for the Central Andes. *Geochem. Geophys. Geosyst.* **2,** doi:10.1029/2001GC000191 (2001).
15. Gagnon, K., Chadwell, C. D. & Norabuena, E. Measuring the onset of locking in the Peru-Chile trench with GPS and acoustic measurements. *Nature* **434,** 205–208 (2005).
16. Dorbath, L., Cisternas, A. & Dorbath, C. Quantitative assessment of great earthquakes in Peru. *Bull. Seismol. Soc. Am.* **80,** 551–576 (1990).
17. Freed, A. M., Burgmann, R., Calais, E., Freymueller, J. & Hreinsdottir, S. Implications of deformation following the 2002 Denali, Alaska, earthquake for postseismic relaxation processes and lithospheric rheology. *J. Geophys. Res.* **111,** doi:10.1029/2005JB003894 (2006).
18. Okada, Y. Internal deformation due to shear and tensile faults in a half-space. *Bull. Seismol. Soc. Am.* **82,** 1018–1040 (1992).
19. Kositsky, A. P. & Avouac, J.-P. Inverting geodetic time series with a principal component analysis-based inversion method. *J. Geophys. Res.* **115,** doi:10.1029/2009JB006535 (2010).
20. Perfettini, H. & Avouac, J.-P. Postseismic relaxation driven by brittle creep: a possible mechanism to reconcile geodetic measurements and the decay rate of aftershocks, application to the Chi-Chi earthquake, Taiwan. *J. Geophys. Res.* **109,** doi:10.1029/2003JB002488 (2004).
21. Hearn, E., Burgmann, R. & Reilinger, R. Dynamics of Izmit earthquake postseismic deformation and loading of the Duzce earthquake hypocenter. *Bull. Seismol. Soc. Am.* **92,** 172–193 (2002).
22. Perfettini, H., Avouac, J.-P. & Ruegg, J. Geodetic displacements and aftershocks following the 2001, $M_w$ = 8.4 Peru earthquake: implications for the mechanics of the earthquake cycle along subduction zones. *J. Geophys. Res.* **109,** doi:10.1029/2004JB003522 (2005).
23. Johnson, K., Burgmann, R. & Larson, K. Frictional properties on the San Andreas fault near Parkfield, California, inferred from models of afterslip following the 2004 earthquake. *Bull. Seismol. Soc. Am.* **96,** S321–S338 (2006).
24. Perfettini, H. & Avouac, J.-P. Modelling afterslip and aftershocks following the 1992 Landers earthquake. *J. Geophys. Res.* **112,** doi:10.1029/2006JB004399 (2007).
25. Baba, T., Hirata, K., Hori, T. & Sakaguchi, H. Offshore geodetic data conductive to the estimation of the afterslip distribution following the 2003 Tokachi-Oki earthquake. *Earth Planet. Sci. Lett.* **241,** 281–292 (2006).
26. Benioff, H. Earthquakes and rock creep. Part I: Creep characteristics of rocks and the origin of aftershocks. *Bull. Seismol. Soc. Am.* **41,** 31–62 (1951).
27. Savage, J. & Langbein, J. Postearthquake relaxation after the 2004 *m*6 Parkfield, California earthquake and rate-and-state friction. *J. Geophys. Res.* **113,** doi:10.1029/2008JB005723 (2008).
28. Langer, C. & Spence, W. The 1974 Peru earthquake series. *Bull. Seismol. Soc. Am.* **85,** 665–687 (1995).
29. Pritchard, M. E. *et al.* Geodetic, teleseismic, and strong motion constraints on slip from recent Southern Peru subduction zone earthquakes. *J. Geophys. Res.* **112,** doi:10.1029/2006JB004294 (2007).
30. Marone, C. Laboratory-derived friction laws and their application to seismic faulting. *Annu. Rev. Earth Planet. Sci.* **26,** 643–696 (1998).


**Supplementary Information** is linked to the online version of the paper at www.nature.com/nature.

**Acknowledgements** We thank J. Freymueller and R. Burgmann for reviews that have helped improve this manuscript. We are grateful to A. Copley for help in editing the manuscript. This study has benefited from support from the Institute de Recherche pour le Développement, the Gordon and Betty Moore Foundation through the Tectonics Observatory, and the National Science Foundation through grant EAR-0838495.

**Author Contributions** H.P. edited the paper and did modelling and field work; J.-P.A. edited the paper and did modelling; H.T. handled the IGP aftershocks data; A.K. did modelling of postseismic deformation; J.-M.N. did the GPS processing; F.B. was in charge of the GPS network; M.C. did modelling of interseismic deformation; A.S. did modelling of the co-seismic deformation; L.A. did field work; D.L.F. did field work, and helped with editing the paper; P.S. helped with logistics.

**Author Information** Reprints and permissions information is available at www.nature.com/reprints. The authors declare no competing financial interests. Readers are welcome to comment on the online version of this article at www.nature.com/nature. Correspondence and requests for materials should be addressed to H.P. (hugo.perfettini@ird.fr).